Rapid Communications

Anomalous Nernst effect and field-induced Lifshitz transition in the Weyl semimetals TaP and TaAs

F. Caglieris,[1] C. Wuttke,[1] S. Sykora,[1] V. Süss,[2] C. Shekhar,[2] C. Felser,[2] B. Büchner,[1,3,4] and C. Hess[1,4]

[1]*Leibniz Institute for Solid State and Materials Research, 01069 Dresden, Germany*

[2]*Max Planck Institute for Chemical Physics of Solids, 01187 Dresden, Germany*

[3]*Institut für Festkörperphysik, TU Dresden, 01069 Dresden, Germany*

[4]*Center for Transport and Devices, TU Dresden, 01069 Dresden, Germany*

(Received 23 May 2018; published 14 November 2018)

The discovery of Weyl fermions in transition-metal monoarsenides/phosphides without inversion symmetry represents an exceptional breakthrough in modern condensed matter physics. However, exploring the inherent nature of these quasiparticles is experimentally elusive because most of the experimental probes rely on analyzing Fermi arc topology or controversial signatures such as the appearance of the chiral anomaly and the giant magnetoresistance. Here, we show that the prototypical type-I Weyl semimetals TaP and TaAs possess a giant anomalous Nernst signal with a characteristic saturation plateau beyond a critical field which can be understood as a direct consequence of the finite Berry curvature originating from the Weyl points. Our results thus promote the Nernst coefficient as an ideal bulk probe for detecting and exploring the fingerprints of emergent Weyl physics.

DOI: 10.1103/PhysRevB.98.201107

Three-dimensional (3D) topological Weyl semimetals (TWSs) [1–7] are characterized by a peculiar electronic structure at half way between a 3D analog of graphene and topological insulators. Indeed, TWSs present bulk Weyl fermions, chiral particles that disperse linearly along all three-momentum directions across the corresponding Weyl points. The Weyl points appear always in pairs, separated in momentum space as a consequence of spin-orbit coupling and breaking of the time-reversal symmetry or inversion symmetry (IS) [8]. Hence, the chiral Weyl fermions experience a finite Berry curvature for which the Weyl points act as a source or sink [3] [Fig. 1(a)]. Recently, intrinsic Weyl states have been observed in transition-metal monoarsenides/phosphides NbP, NbAs, TaP, TaAs, with naturally broken IS [1–7].

The experimental evidence for the presence of Weyl states essentially concerns the investigation of the topological surface state, i.e., the so-called Fermi arcs. More indirect signatures emerge from magnetotransport measurements, which have recently revealed extremely high carrier mobility [9–11] and negative longitudinal magnetoresistance [12–15] in different candidate materials. These have been indeed interpreted as fingerprints of particles with defined chirality, but unfortunately leave room for ambiguity. Since a finite Berry curvature at the Fermi level acts on fermions analogous to a magnetic field, the presence of sizable so-called anomalous transverse transport quantities, viz., the anomalous Hall effect (AHE) and the anomalous Nernst effect (ANE) has been predicted as more direct, unambiguous proof of a finite Berry curvature and thus the existence of Weyl nodes close to the Fermi level [16–21]. Investigating the Nernst effect is particularly interesting for revealing these sought-after anomalous contributions because in ordinary metals its normal contribution vanishes [22–24], in contrast to the Hall effect, where the normal contribution is always finite and scales reciprocally with the carrier density. In this Rapid Communication we show that prototypical Weyl semimetals TaP and TaAs indeed possess a giant anomalous component in the Nernst coefficient S_{xy} with a characteristic saturation plateau beyond a critical magnetic field B_s, which univocally certifies these materials as Weyl semimetals in the bulk. Using a minimal dispersion model of Weyl fermions we explain this unique field dependence as a consequence of a field-induced shift of the chemical potential, resulting in a Lifshitz transition of the particular Fermi-surface sheets which enclose the relevant Weyl points. Taking specific material parameters from band-structure calculations, we estimate B_s in consistency with our experimental results. Our work thus points out the Nernst effect as a smoking-gun experiment for the identification of the emerging Weyl physics in all the candidate materials [7,25–28].

Figure 2(a) shows the experimental data [29] of the magnetic field (B) dependence of the Nernst coefficient normalized to the temperature S_{xy}/T for a single crystal of TaP, in the field range $B = 0$–14 T at selected temperatures. First, the absolute value of S_{xy}/T is large for all the temperatures, reaching the magnitude of what is typically addressed as the "giant" Nernst effect. This represents a strong violation of the so-called Sondheimer's cancellation, which causes the suppression of the Nernst signal in standard single-band materials [30]. Remarkably, for $T = 20$, 30, and 50 K, after an initial increase, S_{xy}/T develops an extended plateau beyond a saturation field $B_s \approx 4$ T, superimposed with quantum oscillations. The establishment of flat plateaus represents a strong departure from the conventional theory of transport, which predicts the normal Nernst coefficient S_{xy}^N evolving directly proportional to the magnetic field B or to its inverse B^{-1} in the low- and high-field limit, respectively [30,31], as reproduced by Eq. (2). The saturating behavior of S_{xy}/T therefore implies the presence of an anomalous, i.e., a magnetic-field-independent component in the Nernst signal. It resembles the behavior of ferromagnetic solids [18,32,33], but is strongly

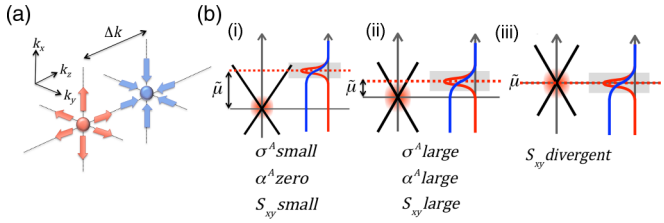

FIG. 1. (a) Schematic picture of the Berry curvature originated from right-handed (blue) and left-handed (red) Weyl points. The Weyl points always appear as a pair with opposite chirality separated by Δk in the k space and they act as a source or sink of Berry curvature (outward or inward arrows). (b) Schematic picture of the folding between the energy-dependent Fermi distribution function (blue) and entropy density (red) with the diverging Berry curvature (red shaded area) near the Weyl point. The gray shaded area marks the thermal energy $k_B T$. The ANE is particularly large and sensitive to a variation of the chemical potential if the gray and red shaded areas overlap, i.e., $\tilde{\mu} \approx k_B T$, which is highlighted in the cases (ii) and (iii).

unusual in nonmagnetic materials with the exception of the Dirac semimetal Cd_3As_2, where similar plateaus have been observed [34].

The inspection of the temperature evolution of the data reveals that such an anomalous component dominates the Nernst effect even up to 50 K. However, for $T = 100$ K, even if the tendency of S_{xy}/T to saturate is still persistent, a constant value is not reached (at least for $B < 14$ T) and for $T = 250$ K the curve is almost completely dominated by a linear component, explainable in terms of a normal contribution according to the semiclassical theory. Interestingly, the crossover between a low-T and a high-T regime, dominated by an anomalous and a normal contribution, respectively, is reproduced in the temperature dependence of S_{xy} for different fields [Fig. 2(b)]. In fact, in these curves S_{xy} shows a broadened maximum at around 80–100 K for high fields which shifts to a lower temperature by decreasing B. We mention that a similar maximum exists also in the analogous compound NbP [35]. However, the characteristic plateaus, which identify the ANE reported here for TaP, do not clearly appear in that case [35].

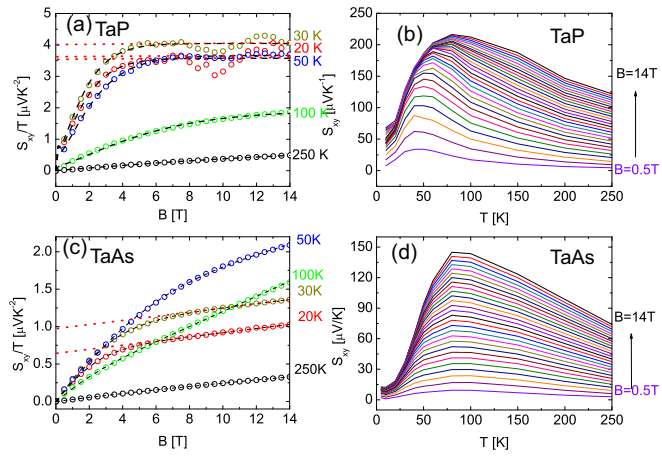

FIG. 2. Nernst effect data for (a), (b) TaP and (c), (d) TaAs. (a) and (c) show the Nernst coefficient normalized to the temperature S_{xy}/T as a function of B. In both of the compounds an anomalous contribution appears as a tendency to saturation. (b) and (d) show the Nernst coefficient S_{xy} as a function of the temperature T. In both compounds we find a crossover between two different temperature regimes which appears as a change of slope with a broadened maximum. The red dotted lines in (a) and (c) represent guides for the eyes. The black dashed lines in (a) and (c) show the results of the phenomenological fit, which well reproduces the experimental data for all the T. Shubnikov–de Haas oscillations appear in the S_{xy}/T vs B curves of TaP at low temperature and they are visible up to 60 K [29].

In analogy to TaP, we performed Nernst measurements on a sample of TaAs. Figure 2(c) shows the B dependence of S_{xy}/T. Unlike the case of TaP, for $T = 20$, 30, and 50 K, the S_{xy}/T vs B curves do not reach a constant value. Even at these low temperatures a B-linear component is apparently overimposed to a large saturating anomalous part, leading to a linear drift of S_{xy}/T instead of a plateau for high fields. Remarkably, this normal contribution becomes already dominant at around 100 K and persists up to 250 K, where the anomalous part is completely unobservable. The difference in the normal component of the Nernst coefficient in the two compounds is not surprising if we consider the strong sensitivity of the conventional Nernst effect even to subtleties of a multiband electronic structure [30].

We extract the qualitative T dependence of the amplitude of the anomalous part of the Nernst coefficient by using a phenomenological model, which decomposes in a normal S^N_{xy} and an anomalous S^A_{xy} contribution [34],

$$S_{xy} = S^N_{xy} + S^A_{xy}, \tag{1}$$

$$S^N_{xy} = S^N_0 \frac{\mu_e B}{1 + (\mu_e B)^2}, \tag{2}$$

$$S^A_{xy} = S^A_0 \tanh(B/B_s), \tag{3}$$

with μ_e the average mobility, S^N_0 and S^A_0 the amplitudes of the normal and the anomalous part, respectively, and B_s the saturation field [34]. The normal contribution as given by Eq. (2) can be derived from the standard theory of transport [31]. We also note that multiband effects can enhance the normal Nernst contribution as a consequence of ambipolar transport but these effects also behave linearly as a function of magnetic field. The field dependence of the anomalous part can be modeled by the empirical formula (3) which is widely accepted to reproduce the saturation effect at high fields [34].

The black dashed lines in Figs. 2(a) and 2(c) show the results of the fit of S_{xy}/T for the sample of TaP and TaAs, respectively. The phenomenological model works well for all T, allowing the isolation of the anomalous component S^A_0. Figure 3 shows the T dependence of S^A_0/T for TaP and TaAs. In both compounds, a rapid decrease of around one order of magnitude indicates the crossover from a low-T to a high-T regime where the anomalous component changes from strong to weak, respectively. The decrease starts at around 150 K for TaP and at around 100 K for TaAs. It is noteworthy that the transition occurs at the same temperature regime that

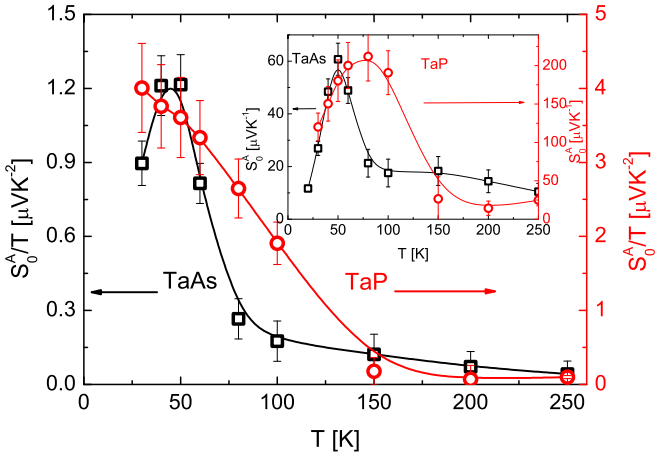

FIG. 3. Temperature dependence of the amplitude of the anomalous part of the Nernst coefficient normalized to the temperature S_0^A/T for TaP (red) and TaAs (black). A crossover between two different regimes is clearly observable in the abrupt change of S_0^A/T that occurs in TaP and TaAs around 150 and 100 K, respectively. Inset: Temperature dependence of S_0^A for TaP (red) and TaAs (black) without temperature normalization. A broadened maximum exists at around $T = 80$ K and $T = 50$ K in TaP and TaAs, respectively.

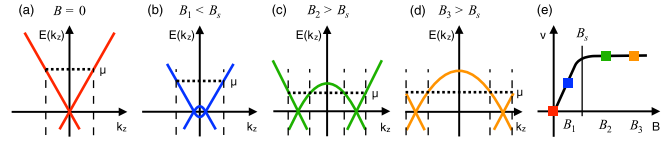

FIG. 4. Schematic behavior of the chemical potential μ in a Dirac/Weyl semimetal. (a) In zero field the energy dispersion shows only one single Dirac node which is placed in the Γ point. (b) Application of magnetic field B leads to the appearance of two nodes whose k-space separation is proportional to B. A shift of μ, indicated by the dotted lines, is induced to conserve the particle number under variation of B. The downshift of μ is responsible for the observed strong variation of the Nernst coefficient for $B < B_s$, where B_s is the saturation field of the Nernst coefficient. (c) For $B > B_s$ a Lifshitz transition occurs and two separated Fermi surfaces appear. (d) By further rising $B > B_s$ the Weyl cone distance increases without changing the k-space volume. Hence, the conservation of the particle number (area between the dashed lines) is already achieved if μ remains almost fixed. As a consequence, the anomalous Nernst coefficient S_{xy}^A will also not change, as highlighted in (e).

characterizes a strong change of the Hall resistivity ρ_{xy} which in both compounds results in a very high average Hall mobility at low T [9–11,36]. This high mobility has been attributed to the suppression of backscattering due to the emergence of Weyl fermions [9–11].

After having established the presence and T dependence of the ANE in TaP and TaAs we turn now to an explanation of the characteristic field-independent plateau in the ANE. The Nernst coefficient $S_{xy} = E_y/(-\nabla_x T)$ can be generally expressed in terms of the thermoelectric tensor α_{ij} and charge conductivity tensor σ_{ij} in the form

$$S_{xy} = \frac{\alpha_{xy}\sigma_{xx} - \alpha_{xx}\sigma_{xy}}{\sigma_{xx}^2 + \sigma_{xy}^2}.$$

It is well established within the Boltzmann approach that anomalous terms proportional to the integrated Berry curvature projected to the direction of the magnetic field (Ω_n^z with n a band index) generally arise in the transverse coefficients [16],

$$\sigma_{xy}^A = \frac{e^2}{\hbar}\sum_n \int \frac{d^3k}{(2\pi)^3}\Omega_n^z(\mathbf{k}) f_{n,\mathbf{k}} \tag{4}$$

$$\alpha_{xy}^A = \frac{k_B e}{\hbar}\sum_n \int \frac{d^3k}{(2\pi)^3}\Omega_n^z(\mathbf{k}) s_{n,\mathbf{k}}. \tag{5}$$

Here, $f_{n,\mathbf{k}} = f(E_{n\mathbf{k}})$ is the Fermi distribution function and $s_{n,\mathbf{k}} = -f_{n,\mathbf{k}} \ln f_{n,\mathbf{k}} - [(1 - f_{n,\mathbf{k}}) \ln(1 - f_{n,\mathbf{k}})]$ the entropy density for the dispersion $E_{n,\mathbf{k}}$ of the conduction electron band n.

A closer analysis of Eqs. (4) and (5) shows that the ANE due to a finite Ω_n^z is large if the energy difference between the chemical potential μ and the Weyl point is of the same order of magnitude or is smaller than the thermal energy $k_B T$ [see cases (ii) and (iii) in Fig. 1(b)] [29]. This is due to the folding of the momentum dependence between the diverging Berry curvature $\Omega_n^z(\mathbf{k})$ and $f_{n,\mathbf{k}}$ (or $s_{n,\mathbf{k}}$) which becomes particularly strong when μ moves towards the Weyl point [37]. The ANE therefore becomes sensitive to both variations of the chemical potential μ and of the temperature T. More specifically, it is expected to grow upon reducing μ as well as upon increasing T from $k_B T \ll \tilde{\mu}$ toward $k_B T \approx \tilde{\mu}$, where $\tilde{\mu}$ measures the distance between the Weyl node and μ.

Magnetic field-induced shift of the chemical potential. Based on a minimal dispersion model for Weyl fermions in a magnetic field, we now argue that the position of the chemical potential is closely related to the B value and also to the topology of the Fermi surface. If a magnetic field is applied to a Dirac or Weyl semimetal with the Dirac or Weyl points in the vicinity of the chemical potential, the latter typically experiences a B-induced shift. This can be inferred from Fig. 4 where for simplicity the effect of a magnetic field applied on a doubly degenerate Dirac cone along the z direction is considered. Figure 4(a) shows the k_z dispersion around a Dirac point for $B = 0$. The chemical potential μ takes a certain position (black dotted horizontal line) above the node, determined by the number of conducting electrons, which corresponds at zero temperature to the number of the occupied states below the Fermi level. The application of a magnetic field along the z direction splits the Dirac cone into two Weyl cones which immediately leads to a finite ANE [Fig. 4(b)]. The magnitude of this ANE remains small as long as $k_B T \ll \tilde{\mu}$ [Fig. 1(b)(i)] [29]. Increasing the magnetic field, however, leads to a further separation of the Weyl nodes where the inevitable downshift of unoccupied states causes a reduction of the chemical potential μ in order to fulfill the condition of a fixed particle number. Thus, the distance between the Weyl points and the chemical potential $\tilde{\mu}$ is reduced, resulting in, as discussed above, an enhancement of the ANE, in agreement with the experiment. For larger fields, μ is pushed to the region where the Weyl cones are separated, such that the Fermi-surface topology has changed

[Fig. 4(c)], leading to the appearance of two distinct Fermi surfaces. In contrast to the behavior at low fields, in this regime the chemical potential remains nearly constant since a further increasing magnetic field simply leads to a further separation of the Weyl nodes but not to a change of the dispersion near the Weyl nodes as sketched in Fig. 4(d). As we will discuss in detail below, this mechanism works also if the starting situation at $B = 0$ is not a degenerate Dirac cone but two preformed Weyl nodes, as in the case of inversion symmetry-breaking TWS, since the driving parameter is the additional shift in momentum space induced by the field and the consequent variation of the k-space volume.

This behavior qualitatively explains the observed saturation of the Nernst coefficient when the magnetic field is larger than some material characteristic value B_s as schematically presented in Fig. 4(e). To compare this scenario with our actual experimental results, we estimate the value of B_s. To this end, we have numerically evaluated μ as a function of B based on the minimal dispersion model $E_{\mathbf{k}} = \pm\sqrt{v_F^2(k_x^2 + k_y^2) + (gB \pm v_F k_z)^2}$ [16]. Specifically, we have calculated the Fermi volume ΔV as a function of μ and B using the integral $\Delta V = \int d^3k f_{\mathbf{k}}(\mu, B)$. Then we have solved the obtained equation numerically for μ leading to a functional relation between μ and B from which we have read off the saturation field B_s defined by constant μ for $B > B_s$. From this approach we find the following relation between B_s, the total Fermi volume ΔV, and the Fermi velocity v_F,

$$B_s = v_F \frac{m_e}{e} \sqrt[3]{\frac{3\Delta V}{2\pi}} 0.745, \tag{6}$$

where m_e denotes the electron mass and e the elementary charge. The number 0.745 in Eq. (6) corresponds to the ratio of the saturated value of the chemical potential compared to its original value, $\mu_s/\tilde{\mu} = 0.745$, where both μ_s and $\tilde{\mu}$ are related to the energy of the Weyl point. For Weyl semimetals such as TaP and TaAs, $\mu_s/\tilde{\mu}$ assumes a material-specific different value of similar magnitude. From band-structure calculations [38] one finds for these materials preformed Weyl points along k_x (with a relative distance Δk_x of the order of 10^{-2} Å^{-1} in the k space). The anomalous S_{xy} measured here has been observed with the magnetic field applied in the z direction, inducing a further separation of the Weyl nodes along k_z, where for both TaAs and TaP $\Delta k_z = 2gB/v_F$ (g is the Landé factor) is of the order of 4×10^{-3} Å^{-1} at $B = 10$ T. Band-structure calculations show that in both materials there are two relevant pairs of Weyl points, usually denoted as W_1 and W_2, which are close to the Fermi level [38]. To obtain our saturation effect at least one pair needs to be enclosed by a nonseparated Fermi surface. In TaP, while W_2 has a separated zero-field Fermi surface, for W_1 the saddle point between the pair of Weyl points is roughly 0.015 eV below the Fermi level ($\tilde{\mu} \approx -0.05$ eV) indicating a nonseparated Fermi surface for $B = 0$. This property allows us to obtain the discussed saturation effect through a shift of the chemical potential at moderate-field values. In the specific situation of TaP the above numbers suggest a somewhat enhanced $\mu_s/\mu = 0.751$ and thus, following Eq. (6), $B_s = 3.3$ T, where $\Delta V \approx 10^{-9}$ Å^{-3} and $v_F \approx 10^5$ m/s have been used as approximate values [38]. For TaAs, on the other hand, for both Weyl points the Fermi surface is already separated according to band-structure calculations. Nevertheless, the described saturation effect is observed also in this material. We attribute this material-specific discrepancy between the experiment and the quantitative predictions to shortcomings of the precision of band-structure calculations. Note that the saddle point energy of W_1 in TaAs is calculated to a value of approximately 0.01 eV which is slightly above the Fermi level. However, a precise description of one-particle states at such small energy leading to the typical small Fermi volumes in TWSs requires an exceptional high k-point sampling in the band-structure calculation. Therefore, we believe that an improvement in such a direction could lead to a correction of the saddle point energy leading to a situation similar to TaP.

Impact of temperature. Due to the broadening of $f_{n,\mathbf{k}}$ (or $s_{n,\mathbf{k}}$), a variation of T instead of μ should also affect the ANE [29]. This effect predicts at low T an enhancement of the ANE with increasing T, which reflects a general property of the Nernst effect, being determined by entropy transport. However, in the case of anomalous transport, the increase is expected to continue upon raising T until close to $k_B T \gg \tilde{\mu}$, where the thermal occupation of the Weyl states at energies above and below the Weyl node is practically the same, resulting in a strong reduction of the ANE [39]. Remarkably, both the low-T increase and the high-T crossover towards smaller values are observed in our experimental results (inset of Fig. 3). In addition, it is worth considering that the high-T reduction of the ANE in TaP occurs at higher T with respect to the case of TaAs. This is consistent with band-structure calculations, which yield a $\tilde{\mu}$ about a factor of 2 larger in TaP as compared to TaAs for the lowest lying Weyl point. This property simulates the influence of the Fermi level with respect to the Weyl points on the anomalous Nernst effect [40].

In conclusion, we reported the observation of a giant ANE in the two Weyl semimetals TaAs and TaP. The occurrence of this ANE can be understood as direct evidence of a large Berry curvature and thus the Weyl points close to the Fermi level, which qualifies the Nernst effect measurements as a valuable tool to elucidate Weyl physics. We have shown that the unique identifying feature of the ANE, viz., the occurrence of field independence beyond a critical field, can be traced back to a strong sensitivity of the ANE to field-induced changes of the chemical potential and a Lifshitz transition due to the separation of the Weyl points in momentum space.

F.C. thanks T. Meng for a discussion about the theory of Weyl semimetals. We thank M. Richter and C. Timm for valuable discussions. This project has been supported by the Deutsche Forschungsgemeinschaft through SFB1143 (Project No. C07). This project has received funding from the European Research Council (ERC) under the European Unions' Horizon 2020 research and innovation programme (Grant Agreement No. 647276-MARS-ERC-2014-CoG).

[1] L. X. Yang, Z. K. Liu, Y. Sun, H. Peng, H. F. Yang, T. Zhang, B. Zhou, Y. Zhang, Y. F. Guo, M. Rahn, D. Prabhakaran, Z. Hussain, S.-K. Mo, C. Felser, B. Yan, and Y. L. Chen, Weyl semimetal phase in the non-centrosymmetric compound TaAs, Nat. Phys. **11**, 728 (2015).

[2] S.-Y. Xu, L. Belopolski, D. S. Sanchez, C. Zhang, G. Chang, C. Guo, G. Bian, Z. Yuan, H. Lu, T.-R. Chang, P. P. Shibayev, M. L. Prokopovych, N. Alidoust, H. Zheng, C.-C. Lee, S.-M. Huang, R. Sankar, F. Chou, C.-H. Hsu, H.-T. Jeng *et al.*, Experimental discovery of a topological Weyl semimetal state in TaP, Sci. Adv. **1**, e1501092 (2015).

[3] H. Weng, C. Fang, Z. Fang, B. A. Bernevig, and X. Dai, Weyl Semimetal Phase in Noncentrosymmetric Transition-Metal Monophosphides, Phys. Rev. X **5**, 011029 (2015).

[4] S.-M. Huang, S.-Y. Xu, I. Belopolski, C.-C. Lee, G. Chang, B. Wang, N. Alidoust, G. Bian, M. Neupane, C. Zhang, S. Jia, A. Bansil, H. Lin, and M. Z. Hasan, A Weyl Fermion semimetal with surface Fermi arcs in the transition metal monopnictide TaAs class, Nat. Commun. **6**, 7373 (2015).

[5] B. Q. Lv, H. M. Weng, B. B. Fu, X. P. Wang, H. Miao, J. Ma, P. Richard, X. C. Huang, L. X. Zhao, G. F. Chen, Z. Fang, X. Dai, T. Qian, and H. Ding, Experimental Discovery of Weyl Semimetal TaAs, Phys. Rev. X **5**, 031013 (2015).

[6] S.-Y. Xu, I. Belopolski, N. Alidoust, M. Neupane, G. Bian, C. Zhang, R. Sankar, G. Chang, Z. Yuan, C.-C. Lee, S.-M. Huang, H. Zheng, J. Ma, D. S. Sanchez, B. Wang, A. Bansil, F. Chou, P. P. Shibayev, H. Lin, S. Jia, and M. Z. Hasan, Discovery of a Weyl fermion semimetal and topological Fermi arcs, Science **349**, 613 (2015).

[7] S.-Y. Xu, N. Alidoust, I. Belopolski, Z. Yuan, G. Bian, T.-R. Chang, H. Zheng, V. N. Strocov, D. S. Sanchez, G. Chang, C. Zhang, D. Mou, Y. Wu, L. Huang, C.-C. Lee, S.-M. Huang, B. Wang, A. Bansil, H.-T. Jeng, T. Neupert *et al.*, Discovery of a Weyl fermion state with Fermi arcs in niobium arsenide, Nat. Phys. **11**, 748 (2015).

[8] Z. K. Liu, L. X. Yang, Y. Sun, T. Zhang, H. Peng, H. F. Yang, C. Chen, Y. Zhang, Y. F. Guo, D. Prabhakaran, M. Schmidt, Z. Hussain, S.-K. Mo, C. Felser, B. Yan, and Y. L. Chen, Evolution of the Fermi surface of Weyl semimetals in the transition metal pnictide family, Nat. Mater. **15**, 27 (2016).

[9] S. Chandra, V. Süss, and M. Schmidt, Mobility induced unsaturated high linear magnetoresistance in transition-metal monopnictides Weyl semimetals, arXiv:1606.06649.

[10] Z. Wang, Y. Zheng, Z. Shen, Y. Lu, H. Fang, F. Sheng, Y. Zhou, X. Yang, Y. Li, C. Feng, and Z.-A. Xu, Helicity-protected ultrahigh mobility Weyl fermions in NbP, Phys. Rev. B **93**, 121112 (2016).

[11] C. Shekhar, A. K. Nayak, Y. Sun, M. Schmidt, M. Nicklas, I. Leermakers, U. Zeitler, Y. Skourski, J. Wosnitza, Z. Liu, Y. Chen, W. Schnelle, H. Borrmann, Y. Grin, C. Felser, and B. Yan, Extremely large magnetoresistance and ultrahigh mobility in the topological Weyl semimetal candidate NbP, Nat. Phys. **11**, 645 (2015).

[12] X. Huang, L. Zhao, Y. Long, P. Wang, D. Chen, Z. Yang, H. Liang, M. Xue, H. Weng, Z. Fang, X. Dai, and G. Chen, Observation of the Chiral-Anomaly-Induced Negative Magnetoresistance in 3D Weyl Semimetal TaAs, Phys. Rev. X **5**, 031023 (2015).

[13] H. Li, H. He, H.-Z. Lu, H. Zhang, H. Liu, R. Ma, Z. Fan, S.-Q. Shen, and J. Wang, Negative magnetoresistance in Dirac semimetal Cd_3As_2, Nat. Commun. **7**, 10301 (2016).

[14] C.-L. Zhang, S.-Y. Xu, I. Belopolski, Z. Yuan, Z. Lin, B. Tong, G. Bian, N. Alidoust, C.-C. Lee, S.-M. Huang, T.-R. Chang, G. Chang, C.-H. Hsu, H.-T. Jeng, M. Neupane, D. S. Sanchez, H. Zheng, J. Wang, H. Lin, C. Zhang *et al.*, Signatures of the Adler–Bell–Jackiw chiral anomaly in a Weyl fermion semimetal, Nat. Commun. **7**, 10735 (2016).

[15] F. Arnold, C. Shekhar, S.-C. Wu, Y. Sun, R. Donizeth dos Reis, N. Kumar, M. Naumann, M. O. Ajeesh, M. Schmidt, A. G. Grushin, J. H. Bardarson, M. Baenitz, D. Sokolov, H. Borrmann, M. Nicklas, C. Felser, E. Hassinger, and B. Yan, Negative magnetoresistance without well-defined chirality in the Weyl semimetal TaP, Nat. Commun. **7**, 11615 (2016).

[16] G. Sharma, P. Goswami, and S. Tewari, Nernst and magnetothermal conductivity in a lattice model of Weyl fermions, Phys. Rev. B **93**, 035116 (2016).

[17] R. Lundgren, P. Laurell, and G. A. Fiete, Thermoelectric properties of Weyl and Dirac semimetals, Phys. Rev. B **90**, 165115 (2014).

[18] W.-L. Lee, S. Watauchi, V. L. Miller, R. J. Cava, and N. P. Ong, Anomalous Hall Heat Current and Nernst Effect in the $CuCr_2Se_{4-x}Br_x$ Ferromagnet, Phys. Rev. Lett. **93**, 226601 (2004).

[19] D. Xiao, Y. Yao, Z. Fang, and Q. Niu, Berry-Phase Effect in Anomalous Thermoelectric Transport, Phys. Rev. Lett. **97**, 026603 (2006).

[20] G. Sharma, C. Moore, S. Saha, and S. Tewari, Nernst effect in Dirac and inversion-asymmetric Weyl semimetals, Phys. Rev. B **96**, 195119 (2017).

[21] Y. Ferreiros, A. A. Zyuzin, and J. H. Bardarson, Anomalous Nernst and thermal Hall effects in tilted Weyl semimetals, Phys. Rev. B **96**, 115202 (2017).

[22] Y. Wang, Z. A. Xu, T. Kakeshita, S. Uchida, S. Ono, Y. Ando, and N. P. Ong, Onset of the vortexlike Nernst signal above T_c in $La_{2-x}Sr_xCuO_4$ and $Bi_2Sr_{2-y}La_yCuO_6$, Phys. Rev. B **64**, 224519 (2001).

[23] K. Behnia, The Nernst effect and the boundaries of the Fermi liquid picture. J. Phys.: Condens. Matter **21**, 113101 (2009).

[24] E. H. Sondheimer, The theory of the galvanomagnetic and thermomagnetic effects in metals, Proc. R. Soc. London, Ser. A **193**, 484 (1948).

[25] Y. Wu, D. Mou, N. H. Jo, K. Sun, L. Huang, S. L. Bud'ko, P. C. Canfield, and A. Kaminski, Observation of Fermi arcs in the type-II Weyl semimetal candidate WTe_2, Phys. Rev. B **94**, 121113 (2016).

[26] K. Deng, G. Wan, P. Deng, K. Zhang, S. Ding, E. Wang, M. Yan, H. Huang, H. Zhang, Z. Xu, J. Denlinger, A. Fedorov, H. Yang, W. Duan, H. Yao, Y. Wu, S. Fan, H. Zhang, X. Chen, and S. Zhou, Experimental observation of topological Fermi arcs in type-II Weyl semimetal $MoTe_2$, Nat. Phys. **12**, 1105 (2016).

[27] S. Khim, K. Koepernik, D. V. Efremov, J. Klotz, T. Förster, J. Wosnitza, M. I. Sturza, S. Wurmehl, C. Hess, J. van den Brink, and B. Büchner, Magnetotransport and de Haas–van Alphen measurements in the type-II Weyl semimetal $TaIrTe_4$, Phys. Rev. B **94**, 165145 (2016).

[28] E. Haubold, K. Koepernik, D. Efremov, S. Khim, A. Fedorov, Y. Kushnirenko, J. van den Brink, S. Wurmehl, B. Büchner, T. K. Kim, M. Hoesch, K. Sumida, K. Taguchi, T. Yoshikawa, A. Kimura, T. Okuda, and S. V. Borisenko, Experimental realization of type-II Weyl state in noncentrosymmetric $TaIrTe_4$, Phys. Rev. B **95**, 241108(R) (2017).

[29] See Supplemental Material at http://link.aps.org/supplemental/10.1103/PhysRevB.98.201107 for details on the sample synthesis, details on thermoelectric measurement setup, the complete set of S_{xy}/T curves, and details on the theoretical model, which includes Refs. [41–43].

[30] K. Behnia and H. Aubin, Nernst effect in metals and superconductors: A review of concepts and experiments, Rep. Prog. Phys. **79**, 046502 (2016).

[31] T. Liang, Q. Gibson, J. Xiong, M. Hirschberger, S. P. Koduvayur, R. J. Cava and N. P. Ong, Evidence for massive bulk Dirac fermions in $Pb_{1-x}Sn_xSe$ from Nernst and thermopower experiments, Nat. Commun. **4**, 2696 (2013).

[32] Y. Pu, D. Chiba, F. Matsukura, H. Ohno, and J. Shi, Mott Relation for Anomalous Hall and Nernst Effects in $Ga_{1-x}Mn_xAs$ Ferromagnetic Semiconductors, Phys. Rev. Lett. **101**, 117208 (2008).

[33] R. Ramos, M. H. Aguirre, A. Anadón, J. Blasco, I. Lucas, K. Uchida, P. A. Algarabel, L. Morellón, E. Saitoh, and M. R. Ibarra, Anomalous Nernst effect of Fe_3O_4 single crystal, Phys. Rev. B **90**, 054422 (2014).

[34] T. Liang, J. Lin, Q. Gibson, T. Gao, M. Hirschberger, M. Liu, R. J. Cava, and N. P. Ong, Anomalous Nernst Effect in the Dirac Semimetal Cd_3As_2, Phys. Rev. Lett. **118**, 136601 (2017).

[35] S. J. Watzman, T. M. McCormick, C. Shekhar, S.-C. Wu, Y. Sun, A. Prakash, C. Felser, N. Trivedi, and J. P. Heremans, Dirac dispersion generates unusually large Nernst effect in Weyl semimetals, Phys. Rev. B **97**, 161404 (2018).

[36] J. Hu, J. Y. Liu, D. Graf, S. M. A. Radmanesh, D. J. Adams, A. Chuang, Y. Wang, I. Chiorescu, J. Wei, L. Spinu, and Z. Q. Mao, π Berry phase and Zeeman splitting of Weyl semimetal TaP, Sci. Rep. **6**, 18674 (2016).

[37] Note that this behavior is a direct consequence of a finite Berry curvature and is not related to the breaking of inversion or time-reversal symmetry.

[38] C.-C. Lee, S.-Y. Xu, S.-M. Huang, D. S. Sanchez, I. Belopolski, G. Chang, G. Bian, N. Alidoust, H. Zheng, M. Neupane, B. Wang, A. Bansil, M. Z. Hasan, and H. Lin, Fermi surface interconnectivity and topology in Weyl fermion semimetals TaAs, TaP, NbAs, and NbP, Phys. Rev. B **92**, 235104 (2015).

[39] Note, however, that at very large temperatures and also in the case where the Weyl point is placed exactly at the Fermi level, corrections to the Boltzmann theory are necessary.

[40] Note that the Weyl points at positive energy can also contribute to the anomalous transport at high T but the same arguments for the reduction of the ANE are also valid there.

[41] R. Kubo, Statistical mechanical theory of irreversible processes, J. Phys. Soc. Jpn. **12**, 570 (1957).

[42] Y. Yao and Z. Fang, Sign Changes of Intrinsic Spin Hall Effect in Semiconductors and Simple Metals: First-Principles Calculations, Phys. Rev. Lett. **95**, 156601 (2005).

[43] M. Gradhand, D. V. Fedorov, F. Pientka, P. Zahn, I. Mertig, and B. L. Györffy, First-principle calculations of the Berry curvature of Bloch states for charge and spin transport of electrons, J. Phys.: Condens. Matter **24**, 213202 (2012).